

Keep it Upright: Model Predictive Control for Nonprehensile Object Transportation with Obstacle Avoidance on a Mobile Manipulator

Adam Heins and Angela P. Schoellig

Abstract— We consider a nonprehensile manipulation task in which a mobile manipulator must balance objects on its end effector without grasping them—known as the *waiter’s problem*—and move to a desired location while avoiding static and dynamic obstacles. In contrast to existing approaches, our focus is on fast online planning in response to new and changing environments. Our main contribution is a whole-body constrained model predictive controller (MPC) for a mobile manipulator that balances objects and avoids collisions. Furthermore, we propose planning using the minimum statically-feasible friction coefficients, which provides robustness to frictional uncertainty and other force disturbances while also substantially reducing the compute time required to update the MPC policy. Simulations and hardware experiments on a velocity-controlled mobile manipulator with up to seven balanced objects, stacked objects, and various obstacles show that our approach can handle a variety of conditions that have not been previously demonstrated, with end effector speeds and accelerations up to 2.0 m/s and 7.9 m/s², respectively. Notably, we demonstrate a projectile avoidance task in which the robot avoids a thrown ball while balancing a tall bottle.

I. INTRODUCTION

We consider the nonprehensile object transportation task known as the *waiter’s problem* [1], which requires the robot to transport objects from one location to another while keeping them balanced on a tray at the end effector (EE), like a restaurant waiter. *Nonprehensile* manipulation [2] refers to the case when the manipulated objects are subject only to unilateral constraints [3] and thus retain some degrees of freedom (DOFs); that is, they are not fully grasped. In contrast to *prehensile* manipulation, a nonprehensile approach allows the robot to carry many objects at once with a simple, non-articulated EE (e.g., a tray; see Fig. 1 and 8). Furthermore, a nonprehensile approach skips the potentially slow grasping and ungrasping processes, and can handle small or delicate objects which cannot be adequately grasped [4]. Beyond food service, efficient object transportation is useful across many industries, such as warehouse fulfilment and manufacturing.

Specifically, we address the waiter’s problem using a velocity-controlled mobile manipulator. Mobile manipulators are capable of performing a wide variety of tasks due to the combination of a large workspace of a mobile base and the manipulation capabilities of robotic arms. We are particularly

The authors are with the Learning Systems and Robotics Lab (www.learnsyslab.org) at the Technical University of Munich, Germany, and the University of Toronto Institute for Aerospace Studies, Canada. They are also affiliated with the University of Toronto Robotics Institute, the Munich Institute of Robotics and Machine Intelligence (MIRMI), and the Vector Institute for Artificial Intelligence. E-mail: adam.heins@robotics.utias.utoronto.ca, angela.schoellig@tum.de

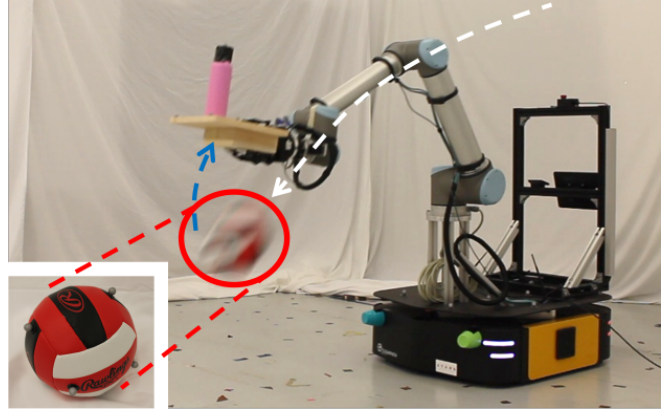


Fig. 1: Our mobile manipulator balancing a pink bottle while avoiding a thrown volleyball (ball circled in red with approximate trajectory in white; approximate end effector trajectory in blue). The controller has less than 0.75 s between first observing the ball and a potential collision. A video of our experiments is available at <http://tiny.cc/keep-it-upright>.

interested in having the mobile manipulator move and react quickly, whether to avoid obstacles or simply for efficiency.

The goal of this work is to develop a controller for a mobile manipulator to quickly transport objects to a desired location without dropping them or colliding with any static or dynamic obstacles, the trajectories of which may not be known a priori. Objects are held on a tray at the EE under frictional contact (i.e., without the use of grasping or adhesive), and they should neither fall over nor slip off the tray. We assume that the geometry, inertial properties, and initial poses of the objects are known, but we do not assume that feedback of the objects’ poses is available online. We assume the robot is velocity-controlled and a kinematic model is available, but its dynamic model is not required.

This work makes the following contributions:

- 1) **Control:** We propose the first full-body model predictive controller (MPC) for a mobile manipulator solving the waiter’s problem. Compared to existing MPC-based approaches to this problem, which have only been demonstrated on fixed-base arms, our controller produces the optimal joint-space trajectory online directly from task-space objectives and constraints, without the use of a higher-level planning step. Furthermore, the controller uses the minimum statically-feasible friction coefficients, which provides robustness to frictional uncertainty, vibration, and other real-world disturbances. When the minimum statically-feasible friction coefficients are zero, we show that the MPC problem can be solved much more efficiently.
- 2) **Experiments:** We present the first demonstrations of

solving the waiter’s problem with a real velocity-controlled mobile manipulator balancing up to seven objects; balancing an assembly of stacked objects; and avoiding static and dynamics obstacles, including a thrown volleyball (see Fig. 1). The EE achieves speeds and accelerations up to 2.0 m/s and 7.9 m/s^2 , respectively.

3) **Code:** Our code is available as an open-source library at <https://github.com/utiasDSL/upright>.

II. RELATED WORK

Prior examples of robots directly inspired by waiters in a restaurant include [5]–[7], but these are mobile robots without manipulator arms. In contrast, we propose to use the high number of DOFs of a mobile *manipulator* for additional objectives like obstacle avoidance. However, the extra DOFs make the control problem more challenging, requiring extra constraints to avoid self-collisions and to ensure that the transported objects stay balanced.

A common approach for balancing objects is to use some manner of sensor feedback to infer the state of objects. In [8], a manipulator performs the classic inverted pendulum task. In [9], a controller is developed to stabilize a tray based on data from an attached accelerometer and gyroscope. In [10], an object is balanced on a tray by a humanoid robot based on force-torque measurements from the robot’s wrists. While the focus of [10] is correcting for an object’s loss of balance, we focus on generating fast motions that *maintain* open-loop balance without object feedback.

A two-dimensional version of the waiter’s problem is addressed in [11], in which a parallel manipulator is mounted on a mobile robot to compensate for the sensed acceleration of the system. The manipulator is controlled to act like a pendulum to minimize the tangential forces acting on a transported object. Simulation of pendular motion has also been used for the slosh-free transport of liquids [12], [13], though these works are focused on imposing particular dynamics on the EE rather than directly constraining object motion. Acceleration constraints are imposed on the EE in [14] to avoid dropping grasped objects or spilling liquids, but nonprehensile object transportation is not addressed.

The waiter’s problem has also been addressed using offline motion planning. Time-optimal path planning (TOPP) approaches minimize the time required to traverse a provided path subject to the constraint that the transported objects remain balanced. In [15], convex programming is used to solve the TOPP problem. In [16], a robust time-scaling approach is used to handle confidence bounds on model parameters like friction, which is combined with iterative learning to learn the bounds. Other planning-based approaches do not assume a path is provided. A kinodynamic RRT-based planner is applied to the nonprehensile transportation task in [4], which demonstrates solving a task where no quasistatic solution exists. An optimization-based planner is applied to the task in [1]. In contrast to these offline planning approaches, our method runs online to react quickly to changes in the environment.

In [17] and [18], a reactive controller automatically regulates the commanded motion to ensure the object remains balanced. A similar approach is applied to legged robots in [19], where the desired trajectory is generated by a spline-based planner. This is one of the only works to use a full mobile manipulator (a quadruped) for the waiter’s problem, but it is demonstrated only in simulation and does not consider dynamic obstacles. To our knowledge, the only physical mobile manipulator experiments for the waiter’s problem have been performed on a humanoid in [20], but similar to [10] they focus on the detection and rejection of disturbances to the object’s stability rather than fast object transportation.

Finally, like us, some recent works use MPC to address the waiter’s problem. In [21], a dual-arm approach is proposed in which a time-optimal trajectory is planned and MPC is used to compute the applied wrench required to realize the object’s trajectory. Another MPC approach is described in [22], which is designed to track a manipulator’s joint-space reference trajectory. In contrast, our approach uses MPC to produce the optimal joint-space trajectory online directly from task-space objectives and constraints, without the use of a higher-level planning step. This allows us to respond quickly to changes in the environment like dynamic obstacles.

III. SYSTEM MODEL

In this section we present the models of the robot and balanced objects.

A. Robot Model

We consider a velocity-controlled mobile manipulator with state $\mathbf{x} = [\mathbf{q}^T, \mathbf{v}^T, \dot{\mathbf{v}}^T]^T$, where \mathbf{q} is the generalized position, which includes the position of the mobile base and the arm’s joint angles, and \mathbf{v} is the generalized velocity. We include acceleration in the state and take the input \mathbf{u} to be jerk to ensure a smooth trajectory.¹ We require only a kinematic model, which we represent generically as

$$\dot{\mathbf{x}} = \mathbf{a}(\mathbf{x}) + \mathbf{B}(\mathbf{x})\mathbf{u}.$$

B. Object Model

We model each object \mathcal{O} as a rigid body subject to the Newton-Euler equations

$$\mathbf{w}_C + \mathbf{w}_{GI} = \mathbf{0}, \quad (1)$$

where \mathbf{w}_C is the total contact wrench and \mathbf{w}_{GI} is the gravito-inertial wrench, expressed in the body frame as

$$\mathbf{w}_{GI} \triangleq \begin{bmatrix} \mathbf{f}_{GI} \\ \boldsymbol{\tau}_{GI} \end{bmatrix} = - \begin{bmatrix} m(\dot{\mathbf{v}}_o - \mathbf{R}_o \mathbf{g}) \\ \mathbf{J} \dot{\mathbf{w}}_o + \boldsymbol{\omega}_o \times \mathbf{J} \boldsymbol{\omega}_o \end{bmatrix},$$

where \mathbf{f}_{GI} and $\boldsymbol{\tau}_{GI}$ are the gravito-inertial force and torque, m is the object’s mass, \mathbf{v}_o and $\boldsymbol{\omega}_o$ are the body-frame linear and angular velocity of the object’s CoM, \mathbf{g} is the gravitational acceleration, and \mathbf{J} is the object’s inertia matrix taken about the CoM. The rotation matrix \mathbf{R}_o represents the object’s

¹While our approach only fundamentally requires reasoning down to acceleration, we found that including jerk for smoothness considerably improves performance on real hardware. We double integrate to obtain velocity commands to send to the actual robot.

orientation with respect to the world and is used to rotate gravity into the body frame.

IV. BALANCING CONSTRAINTS

To control the interaction between the EE and balanced objects in the most general case, we would need to reason about the hybrid dynamics resulting from different contact modes (sticking, sliding, no contact, etc.). Instead, our approach is to enforce constraints that keep the system in a single mode (sticking); that is, we constrain the robot's motion so that the balanced objects do not move with respect to the EE. This is known as a *dynamic grasp* [2]. Now assuming the object is in the sticking mode, we define the object's orientation as $\mathbf{R}_o = \mathbf{R}_e$, such that it is aligned with the EE's orientation \mathbf{R}_e . Furthermore, we have $\mathbf{v}_o = \mathbf{v}_e + \boldsymbol{\omega}_e \times \mathbf{c}$ and $\boldsymbol{\omega}_o = \boldsymbol{\omega}_e$, where \mathbf{v}_e and $\boldsymbol{\omega}_e$ are the EE's linear and angular velocity in the body frame and \mathbf{c} is the position of the object's CoM with respect to the EE. Thus we can write the object's gravito-inertial wrench as

$$\mathbf{w}_{GI} = - \begin{bmatrix} m(\dot{\mathbf{v}}_e - \mathbf{R}_e \mathbf{g}) + m(\dot{\boldsymbol{\omega}}_e^\times + \boldsymbol{\omega}_e^\times \boldsymbol{\omega}_e^\times) \mathbf{c} \\ \mathbf{J} \dot{\boldsymbol{\omega}}_e + \boldsymbol{\omega}_e^\times \mathbf{J} \boldsymbol{\omega}_e \end{bmatrix}, \quad (2)$$

where $(\cdot)^\times$ converts a vector to a skew-symmetric matrix such that $\mathbf{a}^\times \mathbf{b} = \mathbf{a} \times \mathbf{b}$ for any $\mathbf{a}, \mathbf{b} \in \mathbb{R}^3$. We assume that the inertial parameters m , \mathbf{c} , and \mathbf{J} are known. Let us group the remaining variables, along with the EE position \mathbf{r}_e , into the tuple $\mathbf{e} = (\mathbf{R}_e, \mathbf{r}_e, \boldsymbol{\omega}_e, \dot{\boldsymbol{\omega}}_e)$, where $\boldsymbol{\omega}_e = [\mathbf{v}_e^T, \boldsymbol{\omega}_e^T]^T$ is the EE's generalized velocity, which we refer to as the EE state. We can compute \mathbf{e} from the robot state \mathbf{x} via forward kinematics, in which case we may explicitly write $\mathbf{e}(\mathbf{x})$. Furthermore, as can be seen in (2), the object's motion is completely determined by \mathbf{e} when in the sticking mode; the remainder of this section describes the constraints required to maintain the sticking mode. We do not use online feedback of the object state—given the initial object poses with respect to the EE, the controller generates trajectories to keep those poses constant in an open-loop manner.

A. Contact Force Constraints

A general approach for ensuring an object sticks to the EE can be obtained by including all contact forces directly into the optimal control problem and constraining the solution to be consistent with the desired (sticking) dynamics, which has been previously applied to the waiter's problem in e.g. [17]. Consider an arrangement of objects with N total contact points $\{C_i\}_{i \in \mathcal{I}}$ and corresponding contact forces $\{\mathbf{f}_i\}_{i \in \mathcal{I}}$, where $\mathcal{I} = \{1, \dots, N\}$ (see Fig. 2). By Coulomb's law, each contact force \mathbf{f}_i must be inside its friction cone:

$$\|\hat{\mathbf{n}}_i \times \mathbf{f}_i \times \hat{\mathbf{n}}_i\|_2 \leq \mu_i (\hat{\mathbf{n}}_i \cdot \mathbf{f}_i), \quad (3)$$

where $\hat{\mathbf{n}}_i$ is the contact normal and μ_i is the contact's friction coefficient. In practice, an inner linear approximation of (3) is used to improve optimizer convergence, which can be obtained by replacing the L_2 norm with the L_1 norm.

The total contact wrench acting on an individual object is

$$\mathbf{w}_C \triangleq \begin{bmatrix} \mathbf{f}_C \\ \boldsymbol{\tau}_C \end{bmatrix} = \sum_{j \in \mathcal{J}} \begin{bmatrix} \mathbf{f}_j \\ \mathbf{r}_j \times \mathbf{f}_j \end{bmatrix}, \quad (4)$$

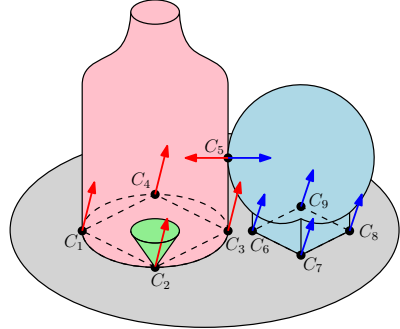


Fig. 2: A bottle (red) and globe (blue) balanced on a tray. This arrangement has a total of $N = 9$ contact points (black dots), with each object having $n = 5$ (C_5 is shared). Contact forces (arrows) at each contact point must belong to their friction cones (one shown in green). The circular contact patch of the bottle is approximated by a quadrilateral. The contact force acting on each object at the shared contact point C_5 must be equal and opposite. If $\mu_i = 0$, the friction cone at C_i collapses to the line along the normal $\hat{\mathbf{n}}_i$.

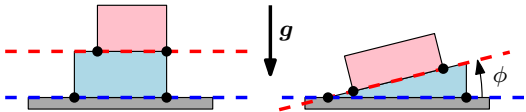


Fig. 3: Planar view of two arrangements of objects, each with two objects balanced on a tray and a total of four contact points (black dots). Left: the support planes (dashed lines) of each object are parallel, so the orientation shown is feasible in the presence of gravity with no friction forces (i.e., we can take $\mu_i = 0$ for all $i \in \mathcal{I}$). Right: the support planes are not parallel, so some friction is always required to balance this arrangement.

where \mathbf{f}_C and $\boldsymbol{\tau}_C$ are the total contact force and torque, $\mathcal{J} \subseteq \mathcal{I}$ is the subset of contact indices for this particular object, and \mathbf{r}_j is the location of C_j with respect to the object's CoM. The object is successfully balanced for a given \mathbf{e} if a set of contact forces can be found each satisfying (3) and consistent with (1), (2), and (4). Surface contacts are represented as polygons with a contact point at each vertex.

However, we need an extra constraint for each contact point shared between two objects (as opposed to contact points between an object and the tray; again refer to Fig. 2): per Newton's third law, the contact force acting on each object must be equal and opposite. Let \mathcal{O}^a and \mathcal{O}^b be two objects in contact at some point C_i , and denote \mathbf{f}_i^a and \mathbf{f}_i^b the corresponding contact forces acting on \mathcal{O}^a and \mathcal{O}^b , respectively. Then we have the constraint

$$\mathbf{f}_i^a = -\mathbf{f}_i^b. \quad (5)$$

To lighten the notation going forward, we gather all contact forces into the vector $\boldsymbol{\xi} = [\mathbf{f}_1^T, \dots, \mathbf{f}_N^T]^T$, and write

$$(\mathbf{e}, \boldsymbol{\xi}) \in \mathcal{B}$$

to indicate that the EE state \mathbf{e} and contact forces $\boldsymbol{\xi}$ together satisfy the balancing constraints (1)–(5) for all objects.

B. Robust Contact Force Constraints

The constraint (3) ensures all contact forces are inside their respective friction cones. However, this assumes accurate knowledge of the friction coefficients, and the constraint may also be violated by unmodelled force disturbances like vibrations and air resistance. To improve the controller's robustness, it is thus desirable for the tangential contact forces

to be small, keeping the forces away from the friction cone boundaries [17]. We propose to plan trajectories using the minimum statically-feasible values of the friction coefficients; that is, the smallest coefficients for which there exists an EE orientation \mathbf{R}_e and contact forces ξ satisfying the balancing constraints with zero EE velocity and acceleration. This ensures that the controller can always converge to a stationary position. Again considering an arbitrary arrangement of objects, we obtain the minimum statically-feasible friction coefficients by solving the optimization problem²

$$\begin{aligned} \operatorname{argmin}_{\mathbf{R}_e, \xi, \{\mu_i\}_{i \in \mathcal{I}}} \quad & \frac{1}{2} \sum_{i \in \mathcal{I}} \alpha_i \mu_i^2 \\ \text{subject to} \quad & \mu_i \geq 0, \quad i \in \mathcal{I} \\ & (\mathbf{e}, \xi) \in \mathcal{B}, \\ & \mathbf{e} = (\mathbf{R}_e, \mathbf{0}, \mathbf{0}, \mathbf{0}), \end{aligned} \quad (6)$$

where $\{\alpha_i\}_{i \in \mathcal{I}}$ are a set of weights. If we have nominal estimates of the friction coefficients $\{\bar{\mu}_i\}_{i \in \mathcal{I}}$, we set each weight $\alpha_i = 1/\bar{\mu}_i$ to lower each coefficient proportionally; otherwise we set $\alpha_i = 1$ for all $i \in \mathcal{I}$. In the common case when the support planes of each object are parallel to each other (see Fig. 3), the solution to (6) is simply $\mu_i = 0$ for all $i \in \mathcal{I}$ with \mathbf{R}_e such that the support planes are orthogonal to gravity. The problem (6) need only be solved once for a given arrangement of objects.

While choosing the minimum friction coefficients may at first appear overly conservative, this approach has a number of benefits. First, it removes the need for accurate friction coefficient estimates, which would require time-consuming physical manipulation of the objects to estimate. Second, *mobile* manipulation can produce significant EE vibration, requiring robust motions to ensure objects are balanced. Third, in the common case when $\mu_i = 0$ for all $i \in \mathcal{I}$, the optimal control problem can be simplified as follows. In general we require one contact force variable $\mathbf{f}_i \in \mathbb{R}^3$ per contact point, each constrained to lie within its (typically linearized) friction cone (3). However, when $\mu_i = 0$, we can parameterize the force with a single scalar $f_i \geq 0$ such that $\mathbf{f}_i = f_i \hat{\mathbf{n}}_i$. This reduces the number of force decision variables by two thirds and replaces the cone constraints by bounds, making the optimization problem faster to solve.

We solved (6) assuming the EE was *stationary*, since we do not assume to know the full EE trajectories a priori. However, in general it is not possible to accelerate multiple objects while assuming *zero* friction, even when there is a feasible stationary solution. To see this, first consider a single object on a tray with its support plane orthogonal to gravity and with $\mu_i = 0$ for all $i \in \mathcal{I}$. From (4) we have $\mathbf{f}_{C_{xy}} = \mathbf{0}$, where the subscript $(\cdot)_{xy}$ denotes the tangential component. Substituting (2) into (1) with $\mathbf{f}_{C_{xy}} = \mathbf{0}$ and dividing out m gives us $[\dot{\mathbf{v}}_e - \mathbf{R}_e \mathbf{g} + (\dot{\boldsymbol{\omega}}_e^\times + \boldsymbol{\omega}_e^\times \boldsymbol{\omega}_e^\times) \mathbf{c}]_{xy} = \mathbf{0}$. So far this is fine: we can plan trajectories that always satisfy this equation.

²It is not necessary to explicitly use a rotation matrix to parameterize orientation in (6): any representation of $SO(3)$ can be used. We use Euler angles. Note also that the balancing constraints are independent of the EE's position, so we set $\mathbf{r}_e = \mathbf{0}$.

However, if we have two objects \mathcal{O}^a and \mathcal{O}^b with CoMs \mathbf{c}^a and \mathbf{c}^b , respectively (e.g., the left arrangement in Fig. 3), then the EE trajectory needs to satisfy *both*

$$[\dot{\mathbf{v}}_e - \mathbf{R}_e \mathbf{g} + (\dot{\boldsymbol{\omega}}_e^\times + \boldsymbol{\omega}_e^\times \boldsymbol{\omega}_e^\times) \mathbf{c}^a]_{xy} = \mathbf{0}, \quad (7)$$

$$[\dot{\mathbf{v}}_e - \mathbf{R}_e \mathbf{g} + (\dot{\boldsymbol{\omega}}_e^\times + \boldsymbol{\omega}_e^\times \boldsymbol{\omega}_e^\times) \mathbf{c}^b]_{xy} = \mathbf{0}, \quad (8)$$

at all times, where the only difference between (7) and (8) is the CoM \mathbf{c} . In general, we cannot find an EE trajectory with non-zero accelerations that always satisfies both equations. However, if there is *some* friction force, the right-hand sides of (7) and (8) are no longer restricted to be identically zero and also need not be equal to each other. Despite this, rather than sacrifice the computational savings of representing each force as a single non-negative scalar, we instead choose to soften the object dynamics constraints (as described in more detail in the following section). This allows tangential contact force to be used when needed, but with a heavy penalty.

V. CONSTRAINED MODEL PREDICTIVE CONTROLLER

We now formulate a model predictive controller to solve the waiter's problem. The controller optimizes trajectories $\mathbf{x}(\tau)$, $\mathbf{u}(\tau)$, and $\xi(\tau)$ over a time horizon $\tau \in [t, t + T]$ by solving a nonlinear optimization problem at each control timestep t . Suppressing the time dependencies, the problem is

$$\begin{aligned} \operatorname{argmin}_{\mathbf{x}, \mathbf{u}, \xi} \quad & \frac{1}{2} \int_{\tau=t}^{t+T} L(\mathbf{x}, \mathbf{u}, \xi) \, d\tau \\ \text{subject to} \quad & \dot{\mathbf{x}} = \mathbf{a}(\mathbf{x}) + \mathbf{B}(\mathbf{x}) \mathbf{u} \quad (\text{system model}) \\ & (\mathbf{e}(\mathbf{x}), \xi) \in \mathcal{B} \quad (\text{balancing}) \\ & \mathbf{0} \leq \mathbf{d}(\mathbf{x}) \quad (\text{collision}) \\ & \underline{\mathbf{x}} \leq \mathbf{x} \leq \bar{\mathbf{x}} \quad (\text{state limits}) \\ & \underline{\mathbf{u}} \leq \mathbf{u} \leq \bar{\mathbf{u}} \quad (\text{input limits}) \end{aligned} \quad (9)$$

where the stage cost is

$$L(\mathbf{x}, \mathbf{u}, \xi) = \|\Delta \mathbf{r}\|_{\mathbf{W}_r}^2 + \|\mathbf{x}\|_{\mathbf{W}_x}^2 + \|\mathbf{u}\|_{\mathbf{W}_u}^2 + \|\xi\|_{\mathbf{W}_f}^2,$$

with $\|\cdot\|_{\mathbf{W}}^2 = (\cdot)^T \mathbf{W} (\cdot)$ for weight matrix \mathbf{W} . The EE position error is $\Delta \mathbf{r} = \mathbf{r}_d - \mathbf{r}_e$, where the desired position \mathbf{r}_d may in general be time-varying or constant; we focus on the latter case to assess the ability of our controller to rapidly move to new positions without a priori trajectory information. The matrices \mathbf{W}_r and \mathbf{W}_x are positive semidefinite; \mathbf{W}_u and \mathbf{W}_f are positive definite. Notice that we do not include a desired orientation: we allow the balancing constraints to handle orientation as needed. If $\mu_i = 0$, then only the normal force f_i is included as a decision variable (as an element of ξ) and (3) is replaced by the constraint $f_i \geq 0$. The vector $\mathbf{d}(\mathbf{x})$ contains the distances between all pairs of collision spheres representing obstacles and the robot body, which must be non-negative to avoid collisions. We discretize (9) with a fixed timestep Δt and solve it online using sequential quadratic programming (SQP) via the open-source framework OCS2 [23]. We use the Gauss-Newton approximation for the Hessian of the cost and we soften all constraints with L_2 penalties [24], which means that the L_2 norm of the constraint violation is penalized in the cost

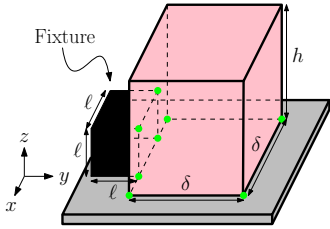


Fig. 4: An arrangement consisting of a red box balanced on a tray along with a black *fixture*, which is rigidly attached to the tray. The fixture adds contact points (shown in green) up the side of the box, which our controller can exploit to accelerate faster.

function. The optimal state trajectory produced by (9) is tracked by a low-level joint controller.

VI. SIMULATION EXPERIMENTS

We begin with simulations to gain insight into the performance of our controller in an idealized environment. We use a simulated version of our experimental platform, a 9-DOF mobile manipulator consisting of a Ridgeback mobile base and UR10 arm, depicted in Fig. 8. In all experiments (simulated and real) we use $\Delta t = 0.1$ s, $T = 2$ s, and weights

$$\begin{aligned} \mathbf{W}_r &= \mathbf{I}_3, & \mathbf{W}_x &= \text{diag}(\mathbf{0}\mathbf{I}_9, 0.1\mathbf{I}_9, 0.01\mathbf{I}_9), \\ \mathbf{W}_u &= 0.001\mathbf{I}_9, & \mathbf{W}_f &= 0.001\mathbf{I}_{\dim(\xi)}, \end{aligned}$$

where \mathbf{I}_n is the $n \times n$ identity matrix. We use a single SQP iteration per control policy update.

A. Balancing Constraint Comparison

We first consider the example shown in Fig. 4, consisting of a box balanced on a tray and in contact with a *fixture*, which is rigidly attached to the tray. We perform experiments with and without the fixture, which is a cube of side length $\ell = 5$ cm. The box has mass $m = 0.5$ kg, height $h = 20$ cm, and a square base with side length $\delta = 6$ cm. The CoM is located at the centroid, the mass distribution is uniform, and $\mu_i = 0.2$ for all $i \in \mathcal{I}$. The task is to move the EE to a desired goal point $\mathbf{r}_d = [-2, 1, 0]^T$ (all desired positions are given in meters relative to the initial EE position) without dropping the box. We compare the trajectories that result from imposing four different sets of balancing constraints:

- **None:** No constraints.
- **Upward:** A constraint to keep the tray oriented upward.
- **Full:** The full set of balancing constraints $(\mathbf{e}, \xi) \in \mathcal{B}$ with each μ_i set to 90% of the true value.³
- **Robust:** The full set of constraints $(\mathbf{e}, \xi) \in \mathcal{B}$ with $\{\mu_i\}_{i \in \mathcal{I}}$ computed using (6). Unless otherwise stated, the solution is $\mu_i = 0$ for all $i \in \mathcal{I}$.

In ideal conditions, the Full and Robust constraints should both keep the objects balanced, but the Full constraints provide less of a safety margin. The Upward approach would work if the motion were quasistatic (i.e., with negligible accelerations), but that would not be fast or reactive.

³We only use 90% of the true (measured or simulated) value to provide some robustness to small constraint violations arising from discretization errors and other numerical disturbances. We subtract a small margin from the support area for the same reason. This is more important in the hardware experiments, where there are more sources of noise and disturbances.

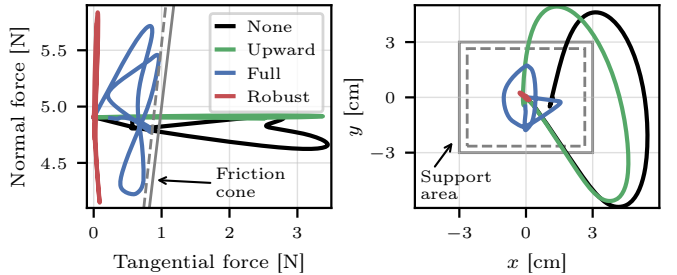


Fig. 5: *Left:* Force applied to the simulated box during motion. *Right:* Corresponding ZMP trajectories. With no constraints (None) or the Upward constraint, the force leaves the friction cone and the ZMP leaves the support area (safety margins in dashed lines), so the box slides and tips over (and is dropped). The Full constraints touch but do not pass the boundaries; the Robust constraints stay far from the boundaries in both cases.

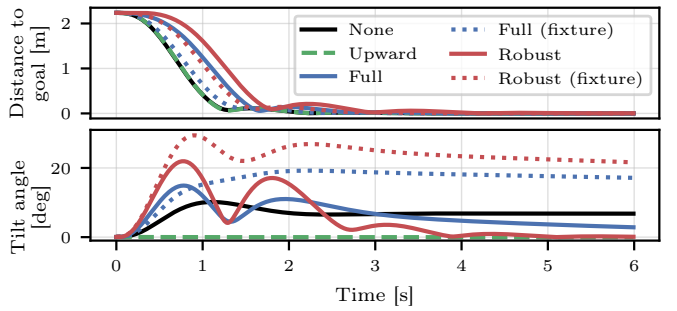


Fig. 6: *Top:* Distance of EE to goal location. *Bottom:* Tilt angle with respect to the upward-pointing (i.e. gravity-aligned) orientation. The Full and Robust constraints limit acceleration to keep the box balanced; the Robust approach also uses higher tilt angles. The None and Upward approaches accelerate faster—and drop the box. When the fixture is added, the Full and Robust constraints can exploit it to achieve convergence speeds more similar to the None and Upward cases. Notice that, except for the Upward constraint, there is no need for the tilt angle to be near zero.

In Fig. 5, the force acting on the object and the zero-moment point (ZMP) are shown relative to the friction cone and support area, respectively. The ZMP is the point about which horizontal moments are zero; if it is outside of the support area, then the object tips. Unsurprisingly, the None and Upward approaches significantly violate both the friction cone and ZMP constraints, resulting in the box being dropped. The Full approach produces motion at the boundary of the constraints but does not violate them, while the Robust approach stays away from the boundaries. In Fig. 6, we see that the robustness of the Robust approach comes at the cost of slower convergence and higher tilt angles compared to the Full approach. When the fixture is added, the Full and Robust approaches can both exploit it to converge nearly as fast as when no constraints are used at all.

B. Non-Parallel Support Planes

Next we show an example when the solution to (6) is not simply $\mu_i = 0$ for all $i \in \mathcal{I}$. The setup consists of a wedge supporting a box at an incline of $\phi = 15^\circ$, similar to the right side of Fig. 3. For simplicity we assume that μ is constant between each pair of objects, so we need only solve (6) for the friction coefficient between the tray and wedge μ_{tw} and between the wedge and box μ_{wb} . We obtain $\mu_{tw} = \mu_{wb} = 0.132$, which corresponds to a tilt angle of $\theta = \arctan(0.132) \approx 7.5^\circ$ relative to the ground for each object,

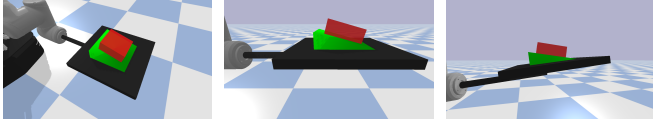


Fig. 7: *Left*: Initial position of wedge (green) and box (red) arrangement. *Middle*: Initial side view. The box is tilted 15° relative to the ground due to the slope of the wedge. *Right*: The position at $t = 6$ s. The controller has oriented the tray so that both the wedge and box are tilted 7.5° relative to the ground, such that each requires as small a μ as possible.

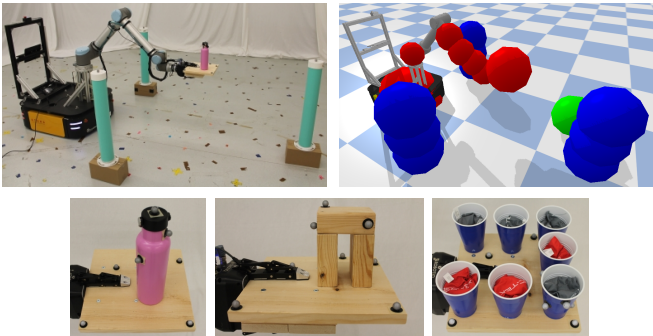


Fig. 8: *Top left*: Real experimental setup. Robot is shown holding the Bottle object. Obstacle locations marked with pylons. *Top right*: Corresponding simulated experimental setup with collision spheres on the robot in red and on the obstacles in blue. *Bottom row*: Bottle, Arch, and Cups object arrangements used for experiments. The arch is an example of non-coplanar contact (the three blocks composing the arch are not attached together). The bottle is filled with sugar and the cups each contain bean bags instead of liquid to avoid spills in the lab.

meaning the wedge and box can be oriented so as to split the angle ϕ between them. Using $\mu_{tw} = \mu_{wb} = 0.132$ for the controller and $\mu_{tw} = \mu_{wb} = 0.2$ for the simulator, we run the simulation with the same goal $\mathbf{r}_d = [-2, 1, 0]^T$. The initial and final configurations are shown in Fig. 7. Note that we need not start in a configuration which the controller thinks is feasible (since the constraints are soft), but the controller will steer toward one over the course of the trajectory. If we were to dispense with (6) and simply try to enforce $\mu_i = 0$ for all $i \in \mathcal{I}$, the controller fails to converge because no feasible stationary solution exists.

VII. HARDWARE EXPERIMENTS

In simulation we gained insight into the behaviour of the controller without the influence of real-world effects like sensor noise or EE vibrations. We now perform experiments on our real mobile manipulator to assess our approach in more realistic scenarios. Position feedback is provided for the arm by joint encoders and for the base by a Vicon motion capture system, which is used in a Kalman filter to estimate the full robot state. We also use motion capture to track the position of the balanced objects, but this information is used only for error reporting. The controller parameters and weights are the same as in the previous section. The controller is run on a standard laptop with eight Intel Xeon CPUs at 3 GHz and 16 GB of RAM. The robot and balanced objects are shown in Fig. 8; the corresponding object parameters are given in Table I. A video of the experiments can be found at <http://tiny.cc/keep-it-upright>.

TABLE I: Approximate parameters for balanced objects shown in Fig. 8. Each contact patch is approximated as a quadrilateral. CoM and inertia are estimated from mass and geometry.

Arrangement	# of objects	# of contacts	Mass per object [g]	Friction coefficients
Bottle	1	4	827	<i>tray-bottle</i> : 0.26
Arch	3	16	180	<i>tray-block</i> : 0.30 <i>block-block</i> : 0.42
Cups	7	28	200	<i>tray-cup</i> : 0.28

A. Static Environments

We perform a large set of experiments with different combinations of objects and desired EE positions, each using the None, Upward, Full, and Robust constraint methods described in the previous section. The desired positions are $\mathbf{r}_{d_1} = [-2, 1, 0]^T$, $\mathbf{r}_{d_2} = [2, 0, -0.25]^T$, and $\mathbf{r}_{d_3} = [0, 2, 0.25]^T$. The object error and controller compute time in an obstacle-free environment are shown in Fig. 9; results for an environment with static obstacles are shown in Fig. 10. We model obstacles as collections of spheres; spheres also surround parts of the robot body for collision checking (see top right of Fig. 8). As expected, the None and Upward approaches almost always fail—the notable exception is for goal \mathbf{r}_{d_2} , which requires more base motion and is thus slower than the other trajectories. The Robust constraints typically produce the lowest object error or are close to it. In general we expect the Robust constraints to have the lowest error, given that they reduce the tangential contact forces and can thus resist unmodelled force disturbances. However, we noticed that the larger tilt angles required by the Robust constraints can occasionally result in some sliding of the objects.

Computationally the Robust constraints scale *much* better with the number of contacts than the Full constraints, since they require less decision variables and use simpler constraints. The Full constraints also require reasonably accurate friction coefficient estimates; the effectiveness of the Robust constraints show that we need not fear frictional uncertainty and (when statically feasible) can set $\mu_i = 0$ for all $i \in \mathcal{I}$ to obtain computational savings. The static obstacle results in Fig. 10 are similar to those for free space except for a modest increase in compute time. Sample trajectories are shown in Fig. 11.

B. Dynamic Environments

We now consider environments that change over time due to dynamic obstacles. Dynamic obstacles are modelled as spheres with known radii, but the controller does not know their trajectories a priori.

1) *An Unexpected Obstacle*: Here we test the controller’s ability to react to unexpected events. We make the controller aware of a new obstacle at varying times t , and the policy must be quickly updated to avoid a collision. The setup is simple: we use the static obstacle environment and goal \mathbf{r}_{d_2} with the Bottle arrangement and a new “virtual” obstacle (the obstacle does not physically exist, but the controller thinks it is present). At time t the new obstacle instantly appears in front of the robot (represented by the green sphere

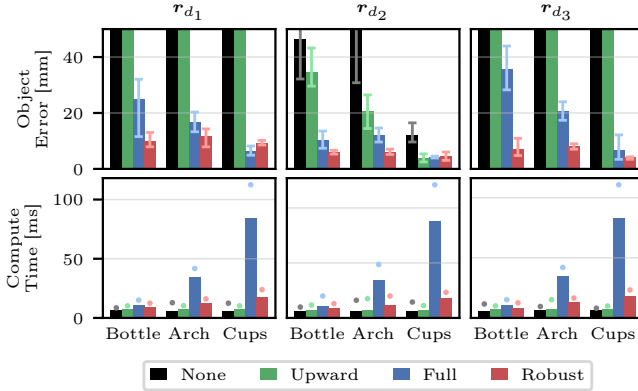


Fig. 9: Object error (top row) and policy compute time (bottom row) for different combinations of objects, goal positions, and constraints in free space. The object error is the maximum distance the object moves from its initial position relative to the tray. In arrangements with multiple objects, only a single object is tracked. The bar shows the average of three runs; the error bars show the minimum and maximum values. The object was completely dropped in all cases where the error extends beyond the axis limits. The compute time is the average amount of time required to compute an updated MPC policy (i.e., one iteration of (9)). The bar is the average across the first 5 s of three runs; the dot shows the maximum value from any of the runs.

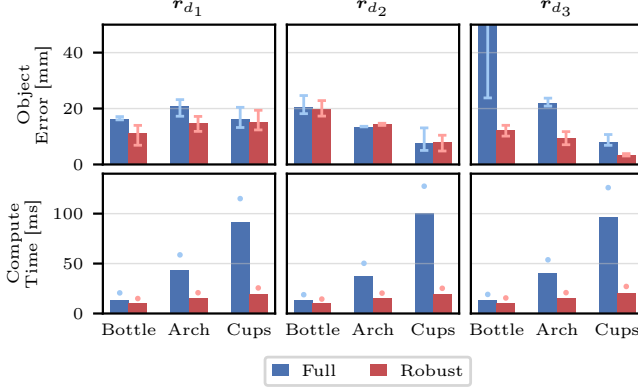


Fig. 10: The same results as shown in Fig. 9 but in an environment with static obstacles and only showing the Full and Robust approaches. Compared to Fig. 9, the errors are similar while the compute times are slightly higher.

in Fig. 8)—imagine a customer in a restaurant suddenly backing out their chair. The results for different t are shown in Fig. 12. The appearance of the obstacle causes significant changes in the trajectory of both the EE and base, but the object is continually balanced despite the sudden change, even when the collision constraint is violated by the obstacle’s appearance. The maximum object error and policy compute time were 18 mm and 23 ms, respectively, across three runs of each of the four obstacle appearance times t . The trajectory with $t = 1$ s achieved the highest EE velocity and acceleration of all our experiments, at 2.0 m/s and 7.9 m/s², respectively.

2) *Projectile Avoidance*: Finally, we consider a ball with position r_b and state $\mathbf{b} = [r_b^T, \dot{r}_b^T]^T$ modelled as a simple projectile with $\ddot{r}_b = \mathbf{g}$. We neglect drag and other possible nonlinear terms, because *avoiding* an object requires a less accurate model than when catching [25] or batting it [26]. The ball is thrown toward the EE, and the robot must move to avoid the objects being hit while also keeping them balanced. For these experiments we use Bottle arrangement and the

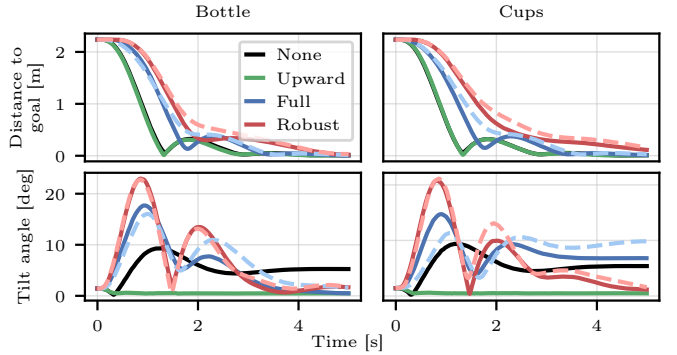


Fig. 11: Samples of trajectories to goal r_d_1 for the Bottle and Cup arrangements with different constraints. Free space results are solid lines; results with static obstacles are dashed. The addition of static obstacles modestly changes the shape of the trajectories. The Full and Robust trajectories differ between the two object arrangements; in particular, notice that Full constraints converge to a much smaller tilt angle with the Bottle compared to the Cups. The Bottle’s higher CoM makes it easier to tip, so it requires a smaller tilt angle when stationary.

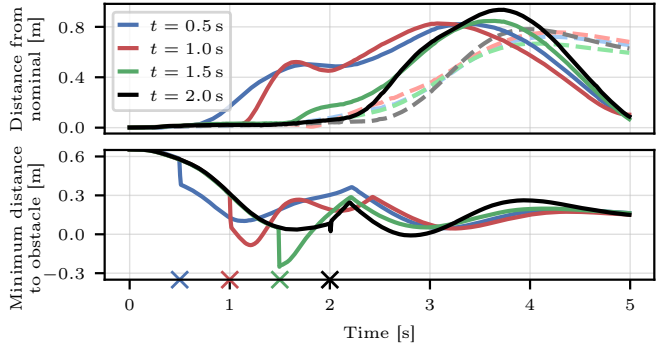


Fig. 12: Top: Distance of EE (solid) and base (dashed) positions from a nominal trajectory with a virtual obstacle suddenly appearing at different times t (also marked with crosses on x -axis). The nominal trajectory has no dynamic obstacle. Bottom: Minimum distance between any collision sphere on the robot and the dynamic obstacle. Notice that in some cases the appearance of the obstacle actually violates the collision constraints, which could also happen with a physical obstacle if the collision sphere was conservatively large. Regardless, the Bottle was never dropped.

Robust constraint method. The controller is provided with feedback of \mathbf{b} once the ball exceeds the height of 1 m; the state is estimated using the motion capture system. The state \mathbf{b} and the projectile dynamics are added to (9) to predict the ball’s motion. We found it more effective to use a form of continuous collision checking in which the controller tries to avoid the entire future *path* of the ball, rather than only avoid its predicted trajectory. Once the ball has passed the EE, the constraint is removed.

The results for 20 throws are shown in Fig. 14. Throws are split evenly between two directions: toward the front of the EE and toward its side. In all cases, the controller has less than 0.75 s to react and avoid the ball. Out of the 20 trials, there is one in which the ball would not have penetrated the collision sphere even if the robot did not move; and (another) one where the bottle was actually dropped. This failure was not due to a collision, but because the bottle tipped over due to the aggressive motion used to avoid the ball. Also notice that the controller does not always completely pull the robot out of collision: there is a trade-off between balancing the object and

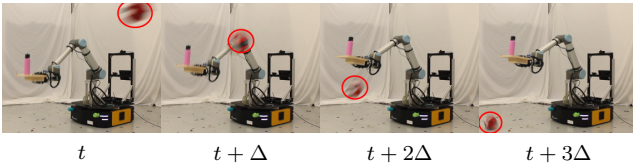


Fig. 13: Example of the robot dodging the volleyball (circled red) while balancing the bottle, with frames spaced by $\Delta = 0.15$ s. Once the ball has passed, the EE moves back to the initial position.

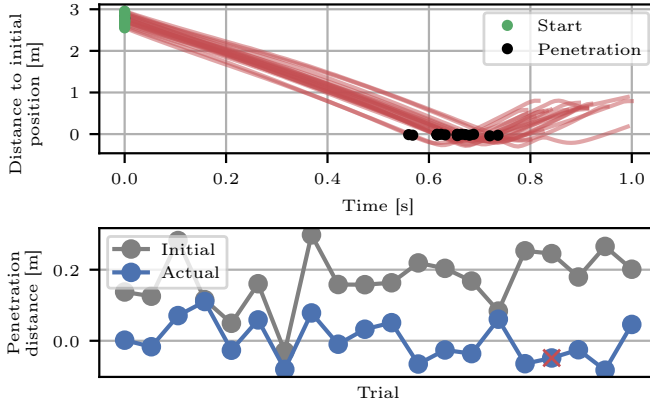


Fig. 14: Top: Distance of projectile to initial EE collision sphere position over time for 20 trials; start is marked in green, initial penetration (i.e., where first collision would occur if the robot did not move) is marked in black. In all cases the controller has less than 0.75 s to react. Bottom: For each trial, maximum penetration distance that would have occurred if the robot did not move (gray) and the actual penetration distance (blue). The single trial where the bottle was dropped is marked with a red cross.

avoiding collision. However, since the collision spheres are conservatively large, we did not experience any failures due to collisions. In these experiments the controller only tries to avoid collisions between the ball and EE; collisions with the rest of the robot's body are not avoided and not considered a failure unless the objects are dropped. In particular, it is possible for the ball to bounce off part of the robot and then hit the balanced objects, but this did not occur during these trials. The maximum object error and policy compute time were 32 mm (ignoring the single failure) and 20 ms, respectively, across the 20 trials.

VIII. CONCLUSION

We presented an MPC-based approach for balancing objects with a velocity-controlled mobile manipulator and demonstrated its performance in simulated and real experiments in a variety of static and dynamic scenarios. In particular, our method is able to react quickly to moving obstacles. We also proposed using minimal values of μ to add robustness to frictional uncertainty and other force disturbances, and demonstrated that this approach is effective and computationally efficient in real-world experiments.

REFERENCES

- [1] F. G. Flores and A. Kecskeméthy, "Time-optimal path planning for the general waiter motion problem," in *Advances in Mechanisms, Robotics and Design Education and Research*, 2013, pp. 189–203.
- [2] K. M. Lynch, "Nonprehensile robotic manipulation: Controllability and planning," Ph.D., Carnegie Mellon University, 1996.
- [3] F. Ruggiero, V. Lippiello, and B. Siciliano, "Nonprehensile dynamic manipulation: A survey," *IEEE Robotics and Automation Letters*, vol. 3, no. 3, pp. 1711–1718, 2018.
- [4] Q.-C. Pham, S. Caron, P. Lertkultanon, and Y. Nakamura, "Admissible velocity propagation: Beyond quasi-static path planning for high-dimensional robots," *Int. J. of Robotics Research*, vol. 36, no. 1, pp. 44–67, 2017.
- [5] B. A. Maxwell *et al.*, "Alfred: The robot waiter who remembers you," in *Proc. AAAI Workshop on Robotics*, 1999, pp. 1–12.
- [6] A. Cheong, M. Lau, E. Foo, J. Hedley, and J. W. Bo, "Development of a robotic waiter system," *IFAC-PapersOnLine*, vol. 49, no. 21, pp. 681–686, 2016.
- [7] A. Y. S. Wan, Y. D. Soong, E. Foo, W. L. E. Wong, and W. S. M. Lau, "Waiter robots conveying drinks," *Technologies*, vol. 8, no. 3, p. 44, 2020.
- [8] B. Sprenger, L. Kucera, and S. Mourad, "Balancing of an inverted pendulum with a SCARA robot," *IEEE/ASME Trans. on Mechatronics*, vol. 3, no. 2, pp. 91–97, 1998.
- [9] T. A. Permadi, J. Halomoan, and S. Hadiyoso, "Balancing system of tray on waiter robot using complementary filter and fuzzy logic," in *Proc. Int. Conf. on Industrial Automation, Information and Communications Technology*, 2014, pp. 15–21.
- [10] J. M. Garcia-Haro, S. Martinez, and C. Balaguer, "Balance computation of objects transported on a tray by a humanoid robot based on 3D dynamic slopes," in *Proc. IEEE-RAS Int. Conf. on Humanoid Robots*, 2018, pp. 1–6.
- [11] A. Dang and I. Ebert-Uphoff, "Active acceleration compensation for transport vehicles carrying delicate objects," *IEEE Trans. on Robotics*, vol. 20, no. 5, pp. 830–839, 2004.
- [12] L. Moriello, L. Biagiotti, C. Melchiorri, and A. Paoli, "Manipulating liquids with robots: A sloshing-free solution," *Control Engineering Practice*, vol. 78, pp. 129–141, 2018.
- [13] R. I. C. Muchacho, R. Laha, L. F. C. Figueiredo, and S. Haddadin, "A solution to slosh-free robot trajectory optimization," in *Proc. IEEE/RSJ Int. Conf. on Intelligent Robots and Systems*, 2022, pp. 223–230.
- [14] J. Ichnowski, Y. Avigal, Y. Liu, and K. Goldberg, "GOMP-FIT: grasp-optimized motion planning for fast inertial transport," in *Proc. IEEE Int. Conf. on Robotics and Automation*, 2022, pp. 5255–5261.
- [15] G. Csorvási, Á. Nagy, and I. Vajk, "Near time-optimal path tracking method for waiter motion problem," *IFAC-PapersOnLine*, vol. 50, no. 1, pp. 4929–4934, 2017.
- [16] J. Luo and K. Hauser, "Robust trajectory optimization under frictional contact with iterative learning," *Autonomous Robots*, vol. 41, no. 6, pp. 1447–1461, 2017.
- [17] M. Selvaggio, J. Cacace, C. Pacchierotti, F. Ruggiero, and P. R. Giordano, "A shared-control teleoperation architecture for nonprehensile object transportation," *IEEE Trans. on Robotics*, vol. 38, no. 1, pp. 569–583, 2022.
- [18] R. Subburaman, M. Selvaggio, and F. Ruggiero, "A non-prehensile object transportation framework with adaptive tilting based on quadratic programming," *IEEE Robotics and Automation Letters*, pp. 1–8, 2023.
- [19] V. Morlando, M. Selvaggio, and F. Ruggiero, "Nonprehensile object transportation with a legged manipulator," in *Proc. IEEE Int. Conf. on Robotics and Automation*, 2022, pp. 6628–6634.
- [20] J. M. Garcia-Haro, "Object oriented control system in humanoid robots for transport tasks," Ph.D., Universidad Carlos III de Madrid, 2019.
- [21] C. Zhou, M. Lei, L. Zhao, Z. Wang, and Y. Zheng, "TOPP-MPC-based dual-arm dynamic collaborative manipulation for multi-object nonprehensile transportation," in *Proc. IEEE Int. Conf. on Robotics and Automation*, 2022, pp. 999–1005.
- [22] V. Morlando, M. Selvaggio, and F. Ruggiero, "Robotic non-prehensile object transportation," in *Proc. Italian Conf. on Robotics and Intelligent Machines*, 2022.
- [23] "OCS2: An open source library for optimal control of switched systems." [Online]. Available: <https://github.com/leggedrobotics/ocs2>
- [24] G. Frison and M. Diehl, "HPIPM: a high-performance quadratic programming framework for model predictive control," *IFAC-PapersOnLine*, vol. 53, no. 2, pp. 6563–6569, 2020.
- [25] K. Dong, K. Pereida, F. Shkurti, and A. P. Schoellig, "Catch the ball: Accurate high-speed motions for mobile manipulators via inverse dynamics learning," in *Proc. IEEE/RSJ Int. Conf. on Intelligent Robots and Systems*, 2020, pp. 6718–6725.
- [26] K. Zhang, Z. Cao, J. Liu, Z. Fang, and M. Tan, "Real-time visual measurement with opponent hitting behavior for table tennis robot," *IEEE Trans. on Instrumentation and Measurement*, vol. 67, no. 4, pp. 811–820, 2018.